Global Scientific JOURNALS

GSJ: Volume 8, Issue 2, February 2020, Online: ISSN 2320-9186

www.globalscientificjournal.com

GEOLOGY AND GEOCHEMISTRY OF MESSONDO BANDED IRON FORMATION-HOSTED IRON ORE FROM THE NORTHWESTERN CONGO CRATON, SOUTHERN CAMEROON: IMPLICATION FOR IRON ORE DEPOSITS

Ndema Mbongué Jean-Lavenir[1,2], Luku Oscar Inyogen[1]

[1] *Department of Geology, University of Buea, P.o. Box 63, Buea, South West region, Cameroon.* E-mail: jndema2012@gmail.com
[2] Laboratory of Petrology and Structural Geology, Department of Earth Sciences, Faculty Sciences, University of Yaoundé I, Cameroon

Key Words
Anoxic conditions, Depleted iron ore, Nyong unit, Silicate facies.

ABSTRACT

Representative BIF samples from Messondo area in the Nyong unit, situated NW corner of the Congo Craton (Ntem complex) in southern Cameroon were analyzed by Inductively Coupled Plasma-Mass Spectrometry (ICP-MS) method to investigate for the origin of iron formations. The Messondo area is made up of metamorphic rocks composed of biotite-gneisses, mylonitic gneisses, amphibolites and banded iron formations (BIFs). The mineral assemblages indicate that biotite-gneisses, mylonitic gneisses and banded iron formations have been metamorphosed under greenschist facies conditions, while amphibolites display a paragenesis of amphibolite facies. The chemical composition of BIFs shows Fe_2O_3 and SiO_2 as the most dominant major elements and the two elements represent 96.7% of the total rock, while the others represent 3.3%, indicating the purity of the chemical precipitates. Trace elements show relative Mn and W enrichments and minor enrichments are observed for transition metals. They are depleted in high field strength elements (HFSE) and enriched in large ion lithophile elements (LILE). The silica contents show that the studied iron formations fall into the group of silicate facies iron deposit, and Fe (26.84-40.50%) concentrations are closer to depleted iron ore (30-50% Fe). The Messondo iron formations are associated to gneisses and amphibolites and have the composition of Fe-sand. Their geochemical signatures indicate that crustal materials contributed insignificantly to the chemical precipitation of the studied iron formation. Messondo iron occurences derive from Precambrian rocks and these rocks were deposited in an oceanic island-arc margin. The Si/Al ratios suggest the hydrothermal origin and all the iron samples fall into the East Pacific Rise Hydrothermal Deposits (EPR) field near the zone defining metalliferous sediments field. The amplitude of the Ce anomaly (0.21 to 1.79) indicates Messondo iron formations into anoxic conditions, while the positive Eu anomaly (Eu/Eu* = 0.29–7.63) suggests that the sources of Fe and Si were derived from deep ocean hydrothermal activity admixing with seawater. The chemical composition of Messondo's iron deposit is closer to the one of Algoma BIF, Lake Superior BIF and Nigeria BIF.

1. INTRODUCTION

Banded iron-formations (BIFs) are marine chemical precipitates that form an integral parts of the preserved Archaean to early Proterozoic sedimentary succession in different part of the world (Klein, 2005; Bhattacharya et al., 2007; Mlsozewska et al., 2012). They consist of alternating silica-rich and iron-rich thin bands or laminated and contain 15% or more iron of sedimentary origin (James, 1954). However and according to (Klein, 2005), typical BIF consists of alternating Si- and Fe-rich layers within an evaluated total Fe and Si contents of 20–40% and 43–56% respectively. Planavsky et al. (2010) proposed the composition-based definition of Fe-formations (IFs) as siliceous and Fe-rich sedimentary chemical precipitates with low levels of detrital siliciclastic or volcaniclastic material (smaller than 1% Al_2O_3) and greater than 10% total Fe, regardless of whether Fe is associated with a carbonate or oxide phase. This definition of Fe formation encompasses both granular and banded Fe formations as well as ferruginous cherts.

Gross (1980) subdivides the IFs into Algoma-type and Lake Superior-type based on their depositional environment. Algoma-type which are small in lateral extent, are interbedded with or stratigraphically associated with volcanic rocks in greenstone belts, and sometimes with volcanogenic massive sulfide deposits (Bekker et al., 2010). Lake Superior-type which are vast, are found in passive margin sedimentary rock sequences and commonly in no association with volcanic rocks (Bekker et al., 2010). This classification also distinguishes banded iron formations (BIFs) from granular iron formations (GIFs) on the base of their structural features. BIFs occur predominantly in Archean to early Paleoproterozoic successions while GIFs are commonly found in Paleoproterozoic sequences (Bekker et al., 2010). James (1954; 1992) subdivide the Lake Superior-type into four facies: sulfide, carbonate, oxide and silicate facies; this is based on the dominant initial iron mineral.

Genetic modelling of Paleoproterozoic BIFs formation has traditionally involved a large variety of diverse processes and attendant major evolutionary changes in the early earth's atmospheric and oceanic composition, from an early anoxic atmosphere dominated by CO_2 and methane to the natural environment we enjoy today, characterized by sufficient oxygen levels to support highly sophisticated multi-cellular life forms (Lyons et al., 2014).

With the high demand for steel worldwide, partly driven by the enormous economic growth currently underway in India and China, exploration for new iron deposits is experiencing a boom, particularly in nonproducing nations such as Cameroon. In Cameroon, the Archaean greenstone belt crops in the southern part of the country within the Ntem complex which corresponds to the northern edge of the Congo craton. The BIFs occurrences within this Precambrian Ntem Complex in southern Cameroon have been widely reported (e.g. Suh et al., 2008; Nforba et al., 2011; Chombong and Suh, 2013; Anderson et al., 2014; Ganno et al., 2015a; 2015b; 2017; 2018; Mbang Banda et al., 2017; Teutsong et al., 2018; Ndime et al., 2018). They are intercalated with metasandstones and metasiltstones (Chombong and Suh, 2013). Although the United Nations Development Programme (UNDP) did a preliminary exploration for itabirite-hosted iron deposits in Cameroon in the 1970s and 1980s, published data on these occurrences are still largely lacking. The aim of this work is to present a description of the geology of the Messondo iron deposits and investigate for the origin of iron formations.

2. GEOLOGIC SETTING

The Messondo area lies within the Paleoproterozoic Nyong unit which belongs to the Ntem Complex (Fig. 1A, 1B). The Ntem Complex is interpreted as the northwestern edge of the Congo Craton in southern Cameroon. The Nyong unit in the NW corner of the Congo craton is a well-preserved granulitic unit of the West Central African Belt resting as an Eburnean nappe on the Congo craton (Toteu et al., 1994; Feybesse et al., 1998). It consists mostly of metasedimentary and metavolcanic rocks, syn-to late-tectonic granitoids and syenites (Toteu et al., 1994; 2001; Pouclet et al., 2007; Ndema Mbongué et al., 2014).

Three groups of ages (Toteu et al., 1994; Lerouge et al., 2006; Lasserre and Soba, 1976; Tchameni et al., 2004) have been recorded in the Nyong unit and they include: (1) Archaean ages (2500–2900 Ma); (2) Palaeoproterozoic (2050 Ma) and (3) Neoproterozoic ages (626 ± 26 Ma). The high-grade metamorphism associated with arrested charnockite formation is dated at 2050 Ma (Toteu et al., 1994). The recent works Ndema Mbongué (2016) indicate that the Palaeoproterozoic ages for the granulitic metamorphism ranged between 1734 ± 22 and 1893 ± 43 Ma (Th-U-Pb EMP-dating on monazites), they are interpreted as the ages of the granulitic metamorphism, contemporaneous with the charnockitization and the emplacement of igneous protoliths. New Pan-African ages for the amphibolite metamorphic facies have been determined and ranged between 577 ± 2 - 677 ± 36 Ma (Th-U-Pb, EMP-dating on monazites; Ndema Mbongué, 2016). These ages correspond to the melt and the emplacement of the sedimentary protoliths. Ages of 1969 ± 170 Ma of charnockites represent the Eburnean cooling (Owona, 2008). This unit includes some Archaean parts of the Ntem complex that were reworked during a Palaeoproterozoic event, and new Palaeoproterozoic material that was accreted to the Archaean craton.

Formerly, the Nyong unit was thought to represent the Neoproterozoic (Pan–African) or the Paleoproterozoic reactivation of the western corner of the Archean Ntem Complex (Lasserre and Soba, 1976; Feybesse et al., 1986). However, the studies of (Toteu et al., 1994; Lerouge et al., 2006) revealed a Paleoproterozoic sedimentation in the unit, which was subsequently thrusted over the Ntem Complex during the Eburnean–Transamazonian orogeny. This orogenic event caused the related plutonism and granulite-facies of the rocks underneath the thrust (Toteu et al., 1994; Lerouge et al., 2006). The main structural characteristic of the Nyong series refers to the Kribi-Campo Shear Zone (KCSZ, Feybesse et al., 1998; Lasserre and Soba, 1976; Maurizot et al., 1986; Madaha Kodjo, 2016), that refers to a Precambrian mega dextral shear zone (Madaha Kodjo, 2016; Kankeu et al., 2017) well studied from Kribi towards the south (Campo).

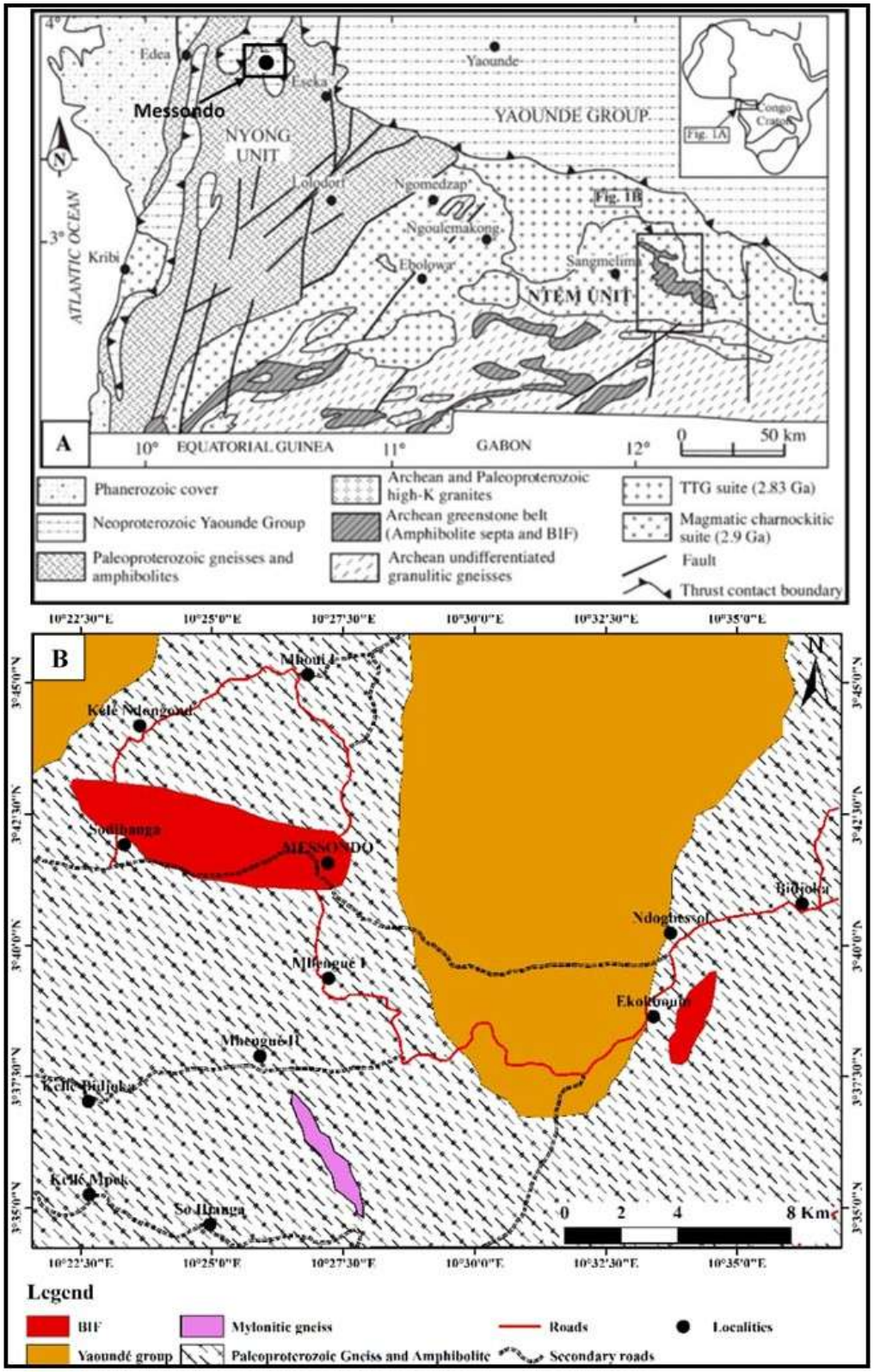

Fig 1. (A) Simplified geologic map of South-West Cameroun (Maurizot et al., 1986), (B) detailed geologic map of Messondo area.

3. METHODS OF INVESTIGATION

The exploration method used in this work is a field survey based on the search and localization of outcrops with the help of the topographic map, and the global positioning system (GPS). 26 representative samples of various rock types were collected in the study area. The samples were collected after every 200-250m. Nine samples were sent to the Institute of Geological Research and Mining (IGRM) laboratory in Yaoundé (Nkolbissong) for the preparation of thin sections. The rocks were cut using a rock cutter in to rectangular cubes (4 × 2.5 × 1 cm) and placed on a glass slide using araldite gum. It is then polished until a thin section of 0.03 mm is reached. The thin sections were later observed using a petrographic microscope in the Geology Laboratory at the Department of Geology in the University of Buea.

Whole rock geochemical analysis was realized on five (05) representative samples of BIFs. Samples were submitted to Activation Laboratories (ACTLABS) in Canada for geochemical analysis following WRA-ICP, analytic code 4B (ACTLABS, 2019). The major elements and trace elements were analyzed by Induction Coupled Plasma - Optical Emission Spectrometry (ICP-OES). Major elements are expressed in percentage dry mass (wt.) with limit detection of 0, 01% and trace elements are expressed in part per million (ppm). Rare earth elements (REE) were analyzed by Inductively Coupled Plasma - Mass Spectrometry (ICP-MS) and are also expressed in part per million (ppm).

4. RESULTS

4.1. Petrography

The study area is made up of metamorphic rocks, they include biotite-gneisses, mylonitic gneisses, amphibolites and BIFs. Mineral abbreviations recommendations by the IUGS Subcommission on the Systematics of Metamorphic Rocks are according to Siivola and Schimid (2007).

4.1.1. Biotite-gneisses

Biotite-gneisses (Fig. 2a) outcrop in the form of slabs and boulders as a light grey rock with medium grained, characterized by alternating of light bands (quartz + feldspar-rich) and ferromagnesian-rich dark bands. Granoblastic microstructure (Fig. 2b) prevails in these rock types. Biotite-gneis samples are composed of subeuhedral, anhedral and ribbon-like quartz (20-25%); subhedral to euhedral plagioclase (20-30%); microcline (20-25%), lamellae and oriented biotite crystals (20-25%) and euhedral to subhedral opaque minerals (≈ 2%). The paragenesis observed in this rock consists of Qtz + Pl + Bt ± Op which corresponds to the greenschist facies.

4.1.2. Mylonitic gneisses

Mylonitic gneisses (Fig. 2c) occur as dome and blocks, they are light in colour and display medium grained. Some samples have a brown-reddish color suggesting that they may contain iron oxides. The rock shows orientation of minerals with alternation of light and dark bands. The light bands consisting of quartz and feldspars are very pronounced while the dark bands are made up of ferromagnesian minerals. Microscopically (Fig. 2d), the rock displays a granoblastic microstructure with major minerals including mosaic and elongated quartz (25-28%), large K-feldspar composed of microcline (30-35%), lenses of plagioclase (20-25%), sheet-like form biotite (15-20%) and muscovite (10-15%). Accessory minerals include opaque oxides (1-3%). The mylonitic gneisses display one paragenesis which is Qtz + Bt + Ms + Pl ± Op, characterizing the greenschist metamorphic facies.

4.1.3. Amphibolites

Amphibolites occur as large blocks or boulders, in slabs or balls. Samples are dark in colour and display fine grained with white patches on their oxidized area and have a low magnetization (Fig. 2e). They also have a granoblastic microstructure (Fig. 2f), and made up of anhedral to subhedral hornblende (30-35%), plagioclase (20-25%) that sometime occur as halo, large and subgrain of quartz (20-23%), orthopyroxene (10-12%), and opaque oxides (5%) as accessory minerals. The single paragenesis of this rock consists of Hbl + Pl + Qtz ± Opx ± Op, characterizing the amphibolite facies.

4.1.4. Banded iron formations (BIFs)

Banded iron formations (BIFs) are reddish-dark massive rocks (Fig. 2g, 2h) showing a strongly magnetic property. They outcrop mainly as blocks and insitu as road cut. The rock is marked by alternating light bands and dark bands. The dark bands mostly composed of magnetite and light band is made up of quartz. Under the microscope, BIFs exhibit granoblastic microstructures made up of euhedral and subhedral-shaped magnetite (45-50%) displaying martitization transformation, quartz (35-40%) defines silica-rich layers of the rock (Fig. 2h), limonite (3%) resulting from the alteration of magnetite. Muscovite (1%) and biotite (3%) appear as accessory phases. The main paragenesis of banded iron formations is Mgt + Qtz + Lm ± Bt ± Ms. This paragenesis characterizes the metamorphism under greenschist facies.

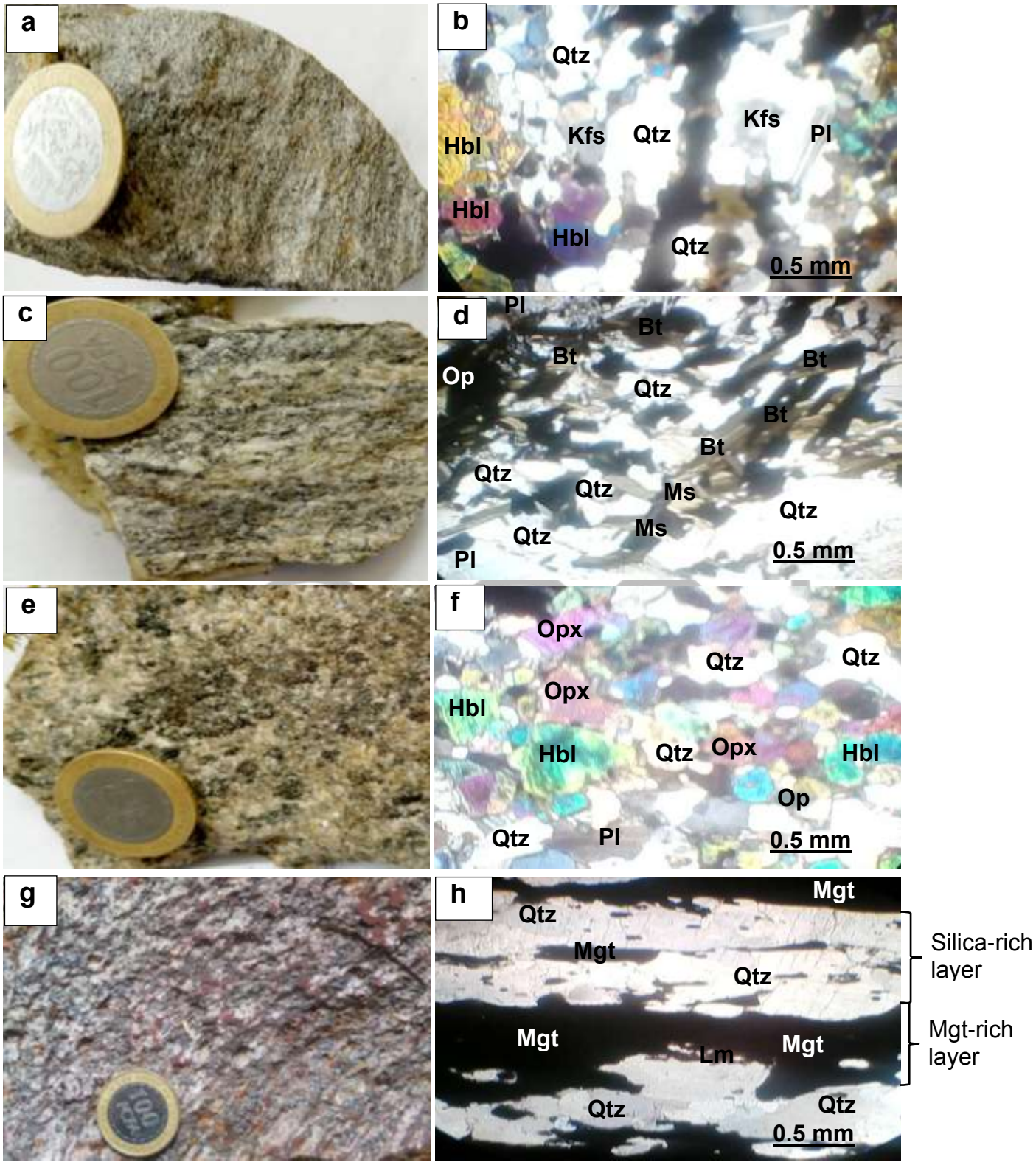

Fig 2. Macro- and microphotographs of various rocks. (a, b): biotite-gneiss; (c, d): mylonitic gneiss; (e, f): amphibolite, (g, h): (BIFs).

4.2. Geochemistry

Whole rock geochemical analysis was realized on five (05) representative samples of banded iron formations and the analytic data are presented in Table 1.

Table 1. Chemical Composition of Messondo BIFs

Elements	SO1	SO2	SO3	ME01	ME02	Mean
SiO_2 (%)	51.41	49.52	57.68	38.25	42.12	47.8
TiO_2	0.12	0.07	0.18	0.06	0.14	0.11
Al_2O_3	1.22	1.56	1.66	0.45	0.72	1.12
Fe_2O_3	38.35	48.69	42.64	57.87	56.96	48.9
MgO	0.19	0.31	0.21	0.14	0.22	0.21
MnO	0.05	0.03	0.07	0.01	0.01	0.03
CaO	0.4	0.01	0.25	0.15	0.2	0.2
Na_2O	0.08	0.05	0.05	0.06	0.05	0.59
K_2O	0.22	0.11	0.01	0.01	0.02	0.07
Cr_2O_5	0.04	0.02	0.05	0.02	0.03	0.03
P_2O_5	0.3	0.14	0.21	0.21	0.23	0.22
LOI	0.27	0.53	-0.34	-1.41	-0.53	-0.3
Total	93.36	101.04	102.67	95.82	100.17	98.61
Na_2O+K_2O	0.3	0.16	0.06	0.07	0.07	0.13
K_2O/Na_2O	2.75	2.2	0.2	0.17	0.4	1.14
Si/Al	42.14	31.74	34.75	85	58.5	50.43
Fe/Ti	319.58	695.57	236.89	964.5	406.86	524.68
Al/Ti	10.17	22.29	9.22	7.5	5.14	10.86
Ag (ppm)	< 0.1	< 0.1	< 0.1	< 0.1	< 0.1	/
As	1.2	1.3	1	< 0.5	0.5	1.17
B	< 20	< 20	< 20	< 20	< 20	/
Bi	< 0.1	< 0.1	< 0.1	< 0.1	< 0.1	/
Cd	< 0.1	< 0.1	< 0.1	< 0.1	< 0.1	/
Co	3.3	1	2.2	2.3	3.1	2.38
Cr	3	4	3	6	5,5	4.3
Cu	8	7	6	5	8	6.8
Ga	< 1	< 1	< 1	5	4	4.5
Hg	0.02	0.02	0.01	0.01	0.02	0.02
Ho	0.1	0.5	0,3	0.2	0.5	0.32
Mn	181	148	156	162	170	163.4
Mo	0.3	0.5	0.42	0.4	0.55	0.43
Ni	1	2	4	3	2	2.4
Pb	4.6	4.1	3.96	0.6	1.3	2.91
Sb	0.6	0.5	0.5	0.2	0.2	0.38

Table 1. Continued

Sc	0.5	1.2	0.96	1.1	1	0.95
Se	0.9	1	0.8	< 0.5	< 0.5	0.95
Sr	4	2	6	15	12	7.8
Th	< 0.1	0,2	0.3	0.5	0.2	0.3
Tl	< 0.1	< 0.1	< 0.1	< 0.1	< 0.1	/
V	3	3	2	6	4	3.6
W	< 0.1	< 0.1	< 0.1	200	200	200
Zn	6	5	6.5	13	11	8.75
La (ppm)	13	8	11	10	11	10.6
Ce	15	25	15	12.1	13	16.02
Pr	3.4	1.3	2.2	17.6	16.9	8.28
Nd	0.8	0.7	0.71	9.5	7.3	3.8
Sm	1.5	2.2	1.2	3.4	3.8	2.42
Eu	2.3	4.3	2.2	0.2	0.4	1.88
Gd	5.4	3.2	3.5	3	2.89	3.6
Tb	0.2	1	0.8	0.3	0.2	0.5
Dy	2.1	0.82	1.3	10.2	10	4.884
Ho	0.5	0.6	0.8	0.1	0.1	0.42
Er	0.4	2.8	1.2	4.1	4.5	2.6
Tm	0.2	0.4	0.2	0.8	1	0.52
Yb	0.2	0.1	0.2	0.3	0.2	0.2
Lu	0.3	0.1	0.2	1.4	1.2	0.64
ΣREE	45.3	50.52	40.51	73	72.49	56.36
(La/Yb)N	4.80	5.91	4.06	2.46	4.06	4.26
(Gd/Yb)N	16.34	19.36	10.59	6.05	8.74	12.22
(Ce/Sm)N	0.70	0.79	0.87	0.25	0.24	0.57
Eu/Eu*	3.81	7.63	5.05	0.29	0.57	3.47
Ce/Ce*	0.52	1.79	0.70	0.21	0.22	0.69
Nd/Nd*	0.07	0.09	0.09	0.25	0.19	0.14

4.2.1. Major elements

The analyses (Table 1) show that, Fe_2O_3 contents vary between 38.35 and 57.87%, with an average of 48.9%. SiO_2 concentrations are elevated and range between 38.25 and 57.68% (average = 47.80%). These two major oxides are the most important components in the Messondo BIFs and they represent 96.7 % of the bulk rock composition. The other major elements (Al_2O_3: 0.72-1.66%; P_2O_5: 0.14-0.3%; CaO: 0.01-0.4%, TiO_2: 0.06-0.18%, MnO: 0.01-0.07% and MgO: 0.14-0.31%) represent 3.3%. These are supported with the petrographic studies where quartz and magnetite are the major minerals observed in the iron samples. Therefore, the major elements chemistry of these iron formations is remarkably with the main constituents being SiO_2 and Fe_2O_3. The high silica contents are also attributable to the high metachert or quartz constituents of the iron formation. Messondo iron formations exhibit a composition of poor-alkali rocks with a total alkali content ($Na_2O + K_2O$) = 0.13%. Based on the diagram log (Fe_2O_{3T}/K_2O) vs. log ($SiO_2/Al2O_3$) after Herron (1988), the studied metasediments (BIFs) have the composition of Fe-sand (Fig. 3).

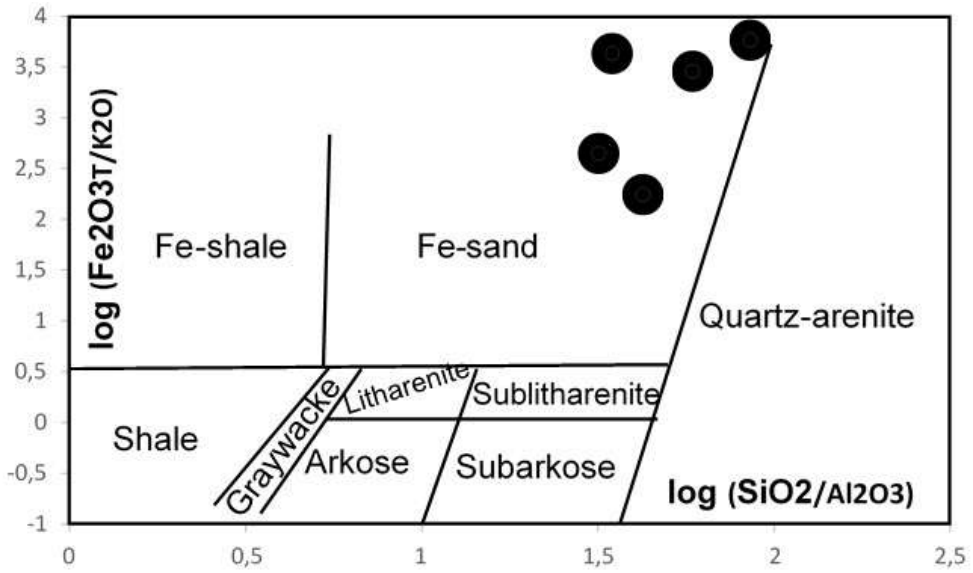

Fig 3. Discriminative log (Fe_2O_{3T}/K_2O) vs. log (SiO_2/Al_2O_3) plot (Herron, 1988) showing the chemical composition of Messondo IFs.

In the correlation matrix (Table 2), Fe_2O_3 shows almost negative correlation with all the major oxides (Fig. 4). Accordingly, Fe_2O_3 shows a high negative correlation (Fig. 4) with SiO_2 (r = -0.87), Cr_2O_3 (r = -0.73) and MnO (r = -0.89). The correlation between Fe_2O_3 and SiO_2 indicates the incorporation of Fe_2O_3 and SiO_2 in different mineral phases. Al_2O_3 contents range between 0.72 and 1.66 % and also show high negative correlation with Fe_2O_3 (r = -0.76). The relative elevated Al_2O_3 and TiO_2 (0.06-0.18%) contents suggest trace inputs of detrital material. Moderated negative correlations are observed between Fe_2O_3 and CaO (r = -0.58), between Fe_2O_3 and Na_2O (r = -0.51) and between Fe_2O_3 and K_2O (r = -0.68; Fig. 4). MgO (r = -0.57) shows negative correlation with CaO, suggesting the incorporation of MgO in carbonate which is present as trace phase in mode. Strong positive correlations are shown between SiO_2 and Al_2O_3 (r = -0.93), SiO_2 and MnO (r = -0.96), SiO_2 and Cr_2O_3 (r = -0.80), and almost positive correlations with all the other oxides (Table 2; Fig. 4). Table 2 also shows a mineral incompatibility between iron and silica. It may be because the mineral did not originate from the same source and as well does not belong to the same mineralogical phase. The positive correlations between the other oxides show that, all these elements are associated to the same mineral phases.

Table 2. Correlation matrix for Messondo iron prospect

	SiO_2	Al_2O_3	Fe_2O_3	MgO	CaO	MnO	K_2O	Na_2O	Cr_2O_3	TiO_2	P_2O_5
SiO_2	1										
Al_2O_3	0.93	1									
Fe_2O_3	-0.7	-0.76	1								
MgO	0.36	0.65	-0.15	1							
CaO	0.31	-0.01	-0.58	-0.57	1						
MnO	0.96	0.82	-0.89	0.10	0.47	1					
K_2O	0.30	0.30	-0.68	0.17	0.43	0.28	1				
Na_2O	0.03	-0.14	-0.51	-0.48	0.73	0.18	0.79	1			
Cr_2O_3	0.80	0.55	-0.73	-0.17	0.69	0.89	0.08	0.17	1		
TiO_2	0.63	0.41	-0.43	-0.04	0.55	0.64	-0.17	-0.14	0.88	1	
P_2O_5	0.06	-0.24	-0.40	-0.62	0.96	0.21	0.46	0.80	0.47	0.37	1

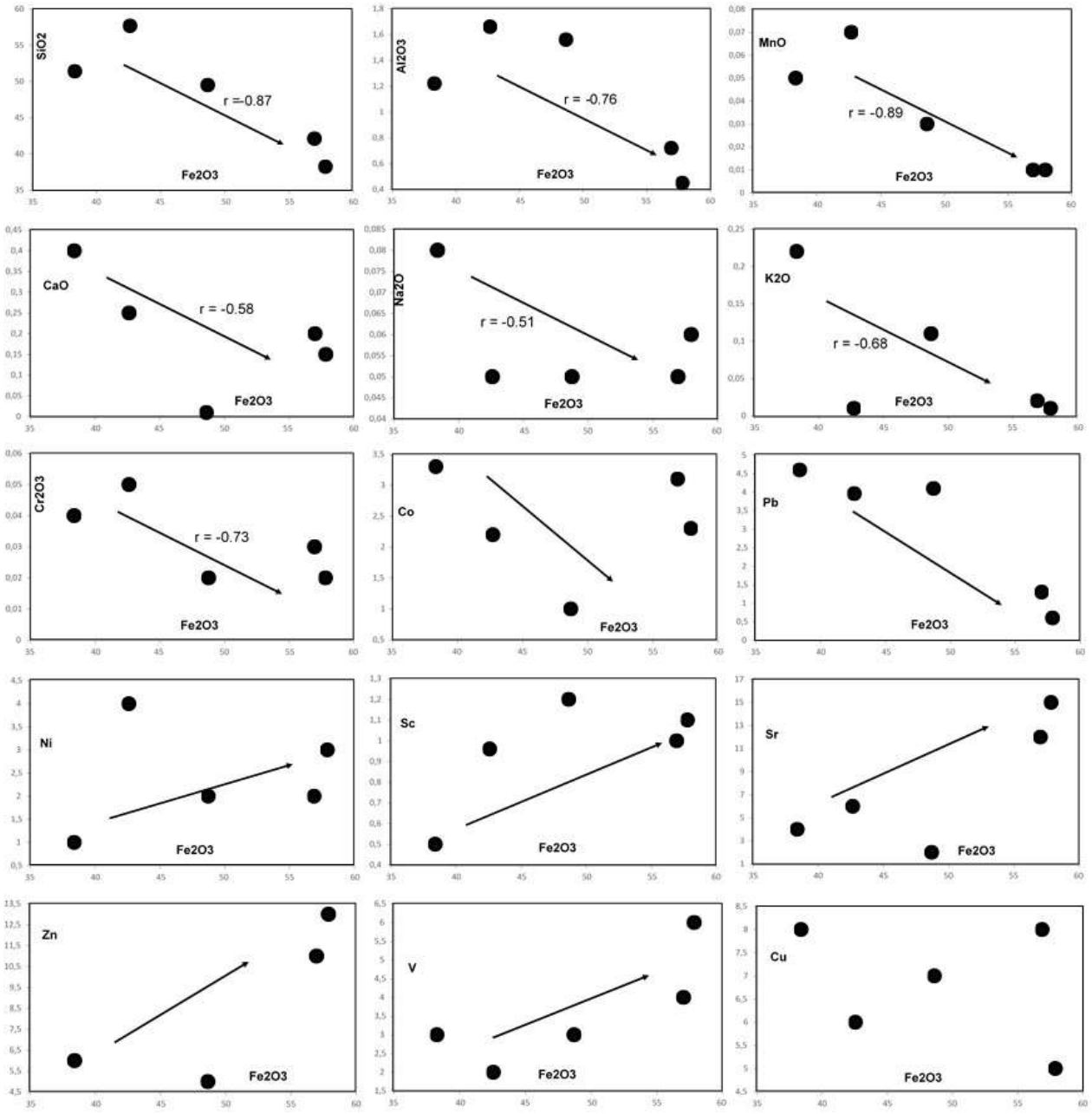

Fig 4. Binary variation plots for major and trace elements in relation to Fe_2O_3.

4.2.2. Trace Elements

Concentrations of trace elements in the bulk samples are shown in Table 1 and no significant enrichments were encountered. Meanwhile Mn (148–181 ppm, av. = 163.4 ppm) shows relative elevated contents. W (200 ppm) contents is almost significant in samples ME01 and ME02 compared with the other samples where W < 0.1 ppm. The studied iron samples are depleted in high field strength elements (HFSE) such as Nb, Th, Pb, REE and enriched in large ion lithophile elements (LILE) like Sr. The trace elements with minor enrichments are transition metals such as Zn (5–11 ppm), Cr (3–6 ppm), V (2–6 ppm), Cu (5–8 ppm) and Pb (0.6–4.6 ppm). These elements are commonly used as indicators of direct volcanogenic hydrothermal input in chemical precipitates (Ganno et al., 2015b). Selected trace elements are plotted against Fe_2O_3 in figure 4. This figure shows that, concentrations of Ni, Sc, Sr, Zn and V increase whereas Co and Pb values decrease with increasing Fe_2O_3 contents. Cu contents is scattered on variation diagrams (Fig. 4). The positive correlations of Fe_2O_3 with Zn and V pointing a hydrothermal source of these metals.

4.2.3. Rare Earth Elements

Rare earth element (REE) distributions in the bulk samples are shown in Table 1. Total REE is low (ΣREE = 40.51-73 ppm, av. = 56.34 ppm) compared with the value of McLennan (1989) that ΣREE = 184.77 ppm. The REE for all samples are normalized to the Post-Archean Australian shale (PAAS; McLennan, 1989). Therefore, chondrite-normalized REE patterns (Fig. 5) are strongly fractionated (La_N/Yb_N = 2.46–5.91) with light earth elements (LREE) enrichment (Ce_N/Sm_N = 0.24–0.87) and heavy rare earth elements (HREE) enrichments (Gd_N/Yb_N = 6.05–19.36). REE patterns also display strong positive Eu anomaly (Eu/Eu* = 0.29–7.63), negative Ce anomaly (Ce/Ce* = 0.21–1.79) and strong negative Nd anomaly (Nd/Nd* = 0.073–0.25).

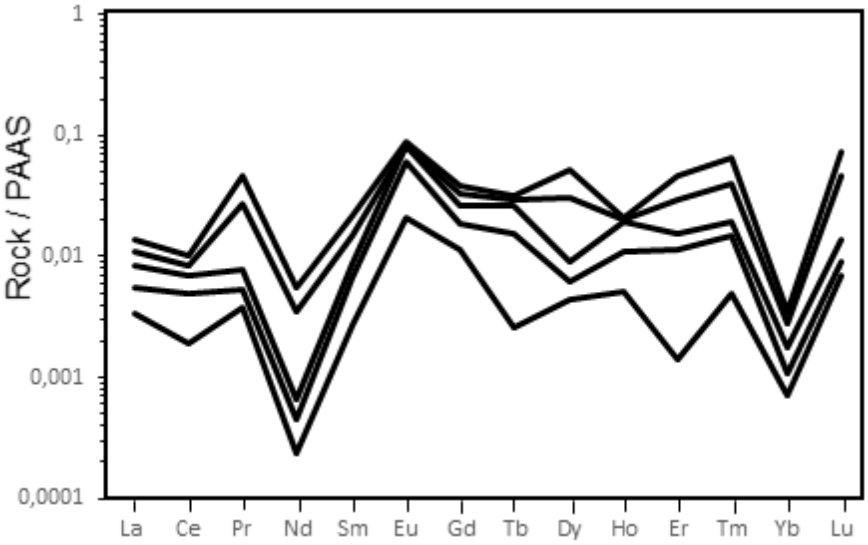

Fig 5. REE patterns for Messondo BIFs.

5. Discussion

5.1. Lithology

The Messondo area is found in the southern part of Cameroon and belongs to the Ntem complex, more precisely in the Nyong series. It made up of banded iron formations, amphibolites, mylonitic gneisses and biotite-gneisses. All these rocks display a granoblastic microstructure. Metzimevin, Meyomessi, Mballam, Nkout, Elom, Kouambo, Gouap and Kpwa-Atog Boga iron ore deposits are well known deposits belonging to the Ntem complex similar to Messondo iron ore deposit. On the petrographic point of view, Mballam iron ore is associated to schists and serpentinites whereas Nkout iron ore is associated to gneisses, charnockites and granites (Suh et al., 2008; Ndime et al., 2018), while Messondo iron formations are associated to gneisses and amphibolites.

5.2. Nature and Protoliths

The studied iron samples have stable features of LILE and their initial geochemical signature can used to identify their protolith. Accordingly, the nature of the sedimentary sources can be constrained using the geochemical signatures of the metasediments. Based on the diagram log (Fe_2O_{3T}/K_2O) vs. log (SiO_2/Al_2O_3) of Herron (1988) represented in figure 3, the studied iron formations have the composition of Fe-sand. This result is different to the one obtained previously by Soh Tamehe et al. (2018) for the Kpwa-Atog Boga iron formations that have Fe-shale and shale to Fe-shale composition.

On the base of silica content (average = 47.80%), the Messondo BIFs fall into the group of silicate facies after James (1954; 1966; 1992). The silicate facies iron deposit is also recorded in Njweng prospect located in the Mbalam iron ore deposit (Ilouga et al., 2013). The Messondo iron deposits are different from those of the Metzimevin (Suh et al., 2008), Nkout (Ndime et al., 2018), Kpwa–Atog Boga (Soh Tamehe et al., 2018), Elom (Ganno et al., 2015b) and Kouambo (Ganno et al., 2017) iron deposits that belong to the oxide facies.

5.3. Source of Iron Silica

The chemical composition of the Messondo iron formations indicates that the major components are SiO_2 and Fe_2O_3, followed by

lesser concentrations of Al_2O_3, TiO_2, MnO, MgO and CaO (Table 1). High contents of SiO_2 and Fe_2O_3 in the studied banded iron-formations indicate the purity of the chemical precipitates. This is in accordance with Cloud (1973) who reported that iron and silica are the principal constituents of BIFs derivate from sea water. Also, REE patterns (Fig. 5) show positive Eu anomaly (Eu/Eu* = 0.29–7.63) suggesting after Klein (2005) and Huston and Logan (2004) that the sources of Fe and Si were derived from deep ocean hydrothermal activity admixing with seawater. The Fe and Mn serve as partial hydrothermal proxies, whereas Al_2O_3 and TiO_2 are usually used as traces for clastic input (Basta et al., 2011; Lan et al., 2014). The presence of Al_2O_3 and TiO_2 indicates after Klein and Beukes (1993) and Manikyamba and Naqvi (1995) that terrigenous clastic materials were involved during the deposition of the Messondo iron formations. The concentrations of HFSE (Nb, Th and Pb) that are typically enriched in chemically evolved crusts are low throughout, which suggests little detrital input during the BIFs precipitation (Pecoits et al., 2009). All of these aforementioned signatures indicate that crustal materials contributed insignificantly to the chemical precipitation of the studied BIFs. Iron formations from Messondo area have Fe concentrations ranging from 26.84 to 40.50%, corresponding to depleted iron ore (30-50% Fe; Morris, 1980). Similar results were obtained from Zambi deposit (Ganno et al., 2015a), Nkout deposit (Ndime et al., 2018) and Kouambo deposit (Ganno et al., 2017).

5.4. Depositional Setting of Metasediments

On an Al_2O_3-SiO_2-Fe_2O_3 ternary diagram (Lepp and Goldich, 1964), studied materials indicate a Precambrian affinity (Fig. 6a). The Precambrian iron formations have low Al_2O_3, TiO_2, P_2O_5, CaO and MgO contents relative to post-Precambrian deposits (Lepp and Goldich, 1964; Govett, 1996). This result coincides with the studies of Mbang Bonda et al. (2017) who also reported a Precambrian affinity for iron mineralization from Edea North area, situated at the West of the study area. The result is also in accordance with Soh Tamahe et al. (2018) indicating the Post Archean sediments in the Kpwa-Atog Boga area metasedimentary rocks. Regarding at the K_2O/Na_2O vs. SiO_2 diagram (Roser and Korsch, 1986) discriminating the tectonic settings (Fig. 6b), most of the samples have been plotted into an oceanic island-arc margin (ARC) field (Fig. 6b), except sample SO1 which fall within the active continental margin (ARM) field. This difference could be explained by the mobility of Na and K. Therefore, the Messondo iron formations are derived from Precambrian rocks, which were deposited in an oceanic island-arc margin (ARC, Fig. 6b). In contrast the Kpwa-Atog Boga metasediments (Soh Tamahe et al., 2018), whose composition ranges from Fe-shale, shale to Fe-shale have been deposited in an active continental margin. Furthermore, some metasedimentary rocks (schists and garnet-rich micaschists) with shale composition deposited in a continental environment have been reported at the Edea–Eseka area within the Nyong unit (Ndema Mbongué et al., 2014). In addition, Chombong et al. (2017) suggested that during the protolith emplacement, there was abundant contribution of continental sediments at the boundary of a shallow basin.

5.5. Origin of Messondo iron mineralization

The Fe- and Si-rich sediments in BIFs are thought to have been derived from a combination of weathering of continental crustal material and venting of submarine hydrothermal fluids (Belevtsev et al., 1982; Hamade et al., 2003). Proposed methods for distinguishing between seawater, hydrothermal, biogenic and detrital sources are based on differences in the mineralogical, chemical and isotopic composition. The Si/Al ratio is used in the study of sedimentary rock to detect eventual hydrogenous, respectively hydrothermal material supply. Based on Toth (1980), hydrothermal origin is characterized by Si/Al > 5.1 while hydrogenous origin has low Si/Al content (Si/Al ≈ 3). The average Si/Al ratio of the Messondo iron mineralization is 50.43 pointing to the hydrothermal origin for the studied iron deposits (Fig. 6c). The hydrothermal origin for the analysed iron rock samples is confirmed with their plotting in the hydrothermal field of the Si vs. Al discrimination diagram (Fig. 5) of Choi and Hariya (1982). The hydrothermal origin of BIFs is also reported in Kpwa–Atog Boga (Soh Tamahe et al., 2018), Gouap (Soh Tamahe et al., 2019), Elom (Ganno et al., 2015b), Zambi (Ganno et al., 2015a), Kouambo (Ganno et al., 2017), Meyomessi (Ganno et al., 2018) and Bienkop (Ilouga et al., 2017). Meanwhile, Suh et al. (2008) suggested that the Metzimevin iron deposit is the result of hypogene leaching of gangue minerals from, and further hematitization of, an itabirite protore. According to Marchig et al. (1982), pure hydrothermal deposits contain very little Al and have high Al/Ti ratios. The contamination of such deposits by pelagic and terrigenous deep-sea sediments enriches them in components such as Ti and Al, resulting drastic lowering of the Fe/Ti ratios and increase in the Al/(Al + Fe + Mn) ratio. Similarly, in the Fe/Ti vs. Al/(Al + Fe + Mn) plot (Fig. 6d) after Barrett (1981), the studied iron samples cluster on the East Pacific Rise Hydrothermal deposits (EPR) near the zone defining metalliferous sediments (Mukherjee, 2008). EPR and Red Sea (RS) origin was proposed for Zambi BIFs (Ganno et al., 2015a), Meyomessi (Ganno et al., 2018) and Kpwa-Atog Boga BIFs (Soh Tamahe et al., 2019), while RS origin is reported in Elom (Ganno et al., 2015b).

The Ce anomaly is calculated to investigate for the conditions of the formation of the study iron deposits. The values are plotted on the Ce/Ce* vs. Nd concentrations (Wright et al., 1987) diagram (Fig. 6e). Elderfield and Pagett (1986) set the Ce anomaly division oxic and anoxic conditions, whereas (Wright et al., 1987) on the basis of further evidence shifted this boundary to -0.10. Taking either boundary shows that the investigated iron samples fall into anoxic conditions.

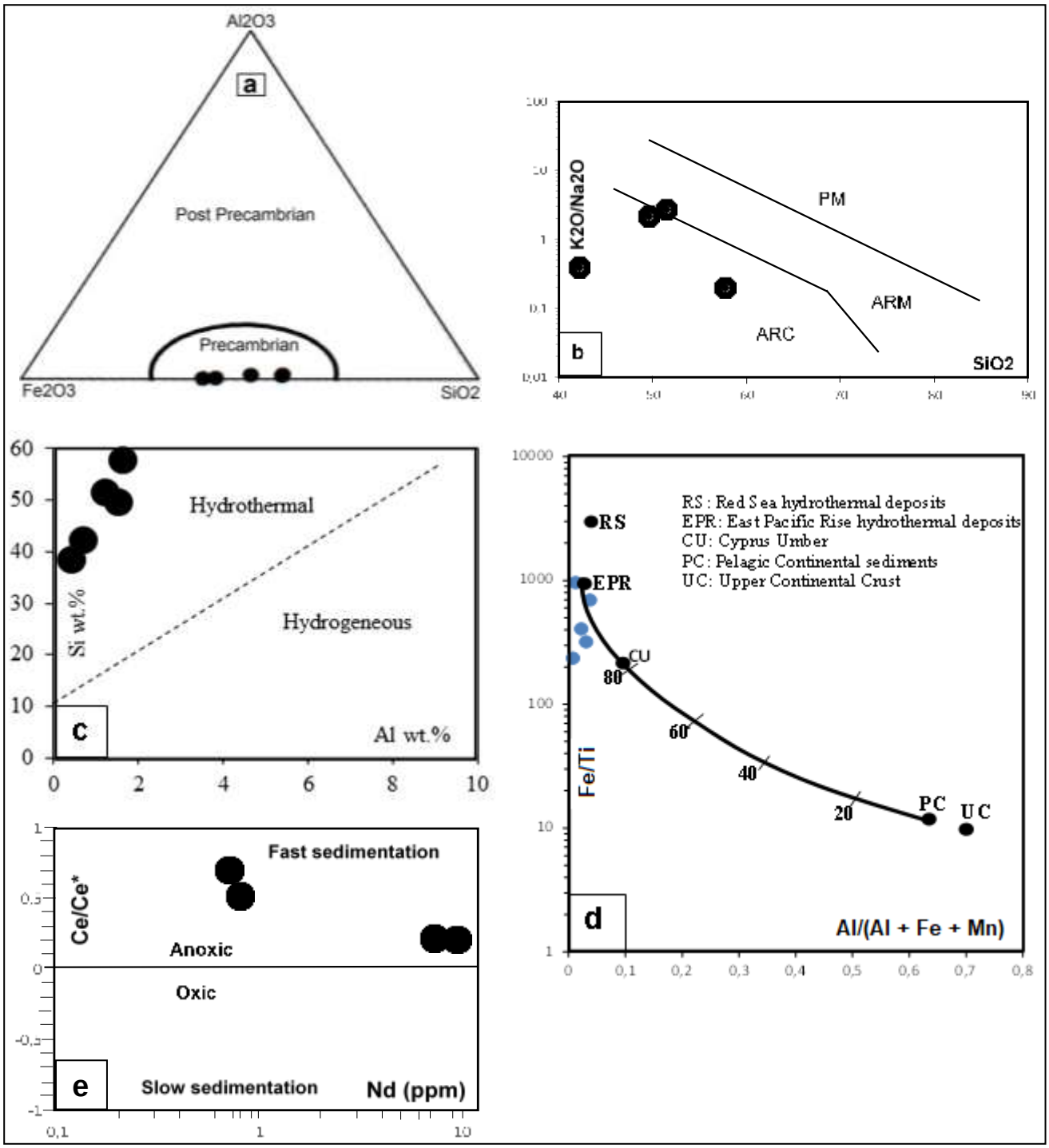

Fig 6. The Messondo iron occurrence composition. (a) After Lepp and Goldich (1964); (b) K_2O/Na_2O vs. SiO_2 diagram according to Roser and Korsch (1986) for discriminating the tectonic settings of the Messondo Bifs: ARC (oceanic island-arc margin), ARM (active continental margin), and PM (passive margin). (c) Discrimination diagram SiO_2 vs. Al_2O_3 after Choi and Hariya (1992) showing the hydrothermal origin of iron mineralization of Messondo area. (d) Fe/Ti versus Al/(Al + Fe + Mn) diagram of Messondo iron-formations, the Messondo iron samples are represented with blue symbols. (e) Plot of Ce anomaly versus Nd concentrations. The dividing line between anoxic and oxic is after Wright et al. (1987).

5.6. Comparison with the others Deposits in the World

The average oxide contents of the banded iron formations from the study area is compared with those of Lake Superior, Algoma and Nigeria. These average contents are recorded in Table 3. When plotted against the respective oxides (Fig. 7), no significant variations are observed: TiO_2, Fe_2O_{3t} and P_2O_5, have relative high proportions while SiO_2 and MnO also have relative low concentrations in Messondo BIFs. Similarities between all the oxides are observed in Messondo iron prospect with other elements (Fig. 7). Messondo's SiO_2 (47.80%) is close to that of the Average Lake Superior BIF (49.13%). The average Fe_2O_{3t} percentage (48.90%) of Messondo is closer to that of the Lake Superior (46.33%).

Table 3. Comparison of major elements of Messondo BIFs with others BIFs around the world.

Samples	Algoma BIF	Lake Superior BIF	Nigeria BIF	Messondo BIF
SiO_2 (%)	50.58	49.13	57.66	47,80
TiO_2	0.09	0.02	0.02	0,11
Al_2O_3	3.06	1.45	0.28	1,12
Fe_2O_{3t}	42.62	46.33	42.02	48,90
MnO	0.14	0.76	0.06	0,03
MgO	1.56	1.29	0.01	0,21
CaO	1.54	1.64	0.02	0,20
Na_2O	0.32	0.12	0.01	0,06
K_2O	0.59	0.15	0.02	0,07
P_2O_5	0.21	0.06	0.05	0,22
S	0.3	0.02	NA	<0.01

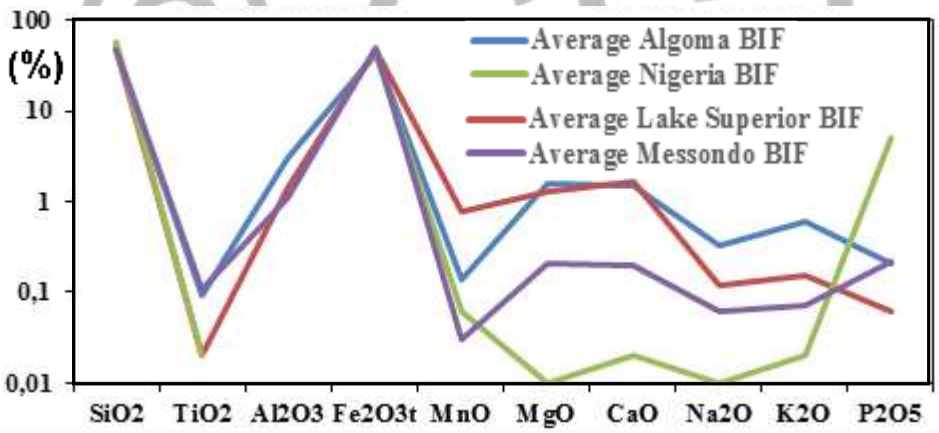

Fig 7. Chemical variation in composition of the major elements of Messondo's BIFs with other BIFs around the world.

6. Conclusion

The Messondo area lies within the Paleoproterozoic Nyong unit which belongs to the Ntem Complex (Congo Craton). It made up of metamorphic rocks composed of biotite-gneisses, mylonitic gneisses, amphibolites and banded iron formations (BIFs). These rocks display granoblastic microstructures. The chemical composition of Messondo iron deposits shows Fe_2O_3 and SiO_2 as the most dominant major elements and the two elements represent 96.7% of the total rock, while the others represent 3.3%, indicating the purity of the chemical precipitates. Trace elements show relative Mn and W enrichments, and minor enrichments are observed for transition metals (Zn, Cr, V, Cu, and Pb). The studied iron formations are depleted in HFSE (Nb, Th, Pb, and REE) and enriched in LILE (Sr). The silica contents show that the studied iron samples fall into the group of silicate facies iron deposit, and the concentrations of Fe (26.84-40.50%) correspond to depleted iron ore (30-50% Fe). The Messondo BIFs are associated to gneisses and amphibolites and have the composition of Fe-sand. The geochemical signatures indicate that crustal materials contributed insignificantly to the chemical precipitation of the studied iron prospect. Messondo iron formations derive from Precambrian rocks and have low Al_2O_3, TiO_2, P_2O_5, CaO and MgO. These rocks were probably deposited in an oceanic island-arc margin. The Si/Al ratios of the studied iron rocks

pointing to the hydrothermal origin and this is supported by the plot of all samples in the East Pacific Rise Hydrothermal Deposits (EPR) near the zone defining metalliferous sediments field. The amplitude of the Ce anomaly (0.21 to 1.79) indicates Messondo iron formations into anoxic conditions, while the observed positive Eu anomaly (Eu/Eu* = 0.29–7.63) suggests that the sources of Fe and Si were derived from deep ocean hydrothermal activity admixing with seawater. The chemical composition of Messondo iron formations is similar with those of Algoma BIF, Lake Superior BIF, and Nigeria BIF.

References

[1] Actlabs, Schedule of Services and Fees, Geochemistry – International. pp. 1-44, 2019, www.actlabs.com
[2] K.F.E. Anderson, F. Wall, G.K. Rollinson, C.J. Moon, "Quantitative mineralogical and chemical assessment of the Nkout iron ore deposit, Southern Cameroon," Ore Geol. Rev. 62, pp. 25–39, 2014
[3] T.J. Barrett, "Chemistry and mineralogy of Jurassic bedded chert overlyingophiolites in the North Appenines, Italy," Chem. Geol. 34, pp. 289–317, 1981
[4] F.F. Basta, A.E. Maurice, L. Fontbote, P. Favarger, "Petrology and geochemistry of the banded iron formation (BIF) of Wadi Karim and Um Anab, Eastern Desert, Egypt: implications for the origin of Neoproterozoic BIF," Precambr. Res. 187, pp. 277–292, 2011
[5] A. Bekker, J.F. Slack, N. Planavsky, B. Krapez, A. Hofmann, K.O. Konhauser, O.J. Rouxel, "Iron formation: the sedimentary product of a complex interplay among mantle, tectonic, oceanic and biospheric processes," Econ. Geol. 105, 467–508, 2010
[6] H.N. Bhattacharya, I. Chakraborty, K.K. Ghosh, "Geochemistry of some banded iron-formations of the Archean supracrustals, Jharkhand–Orissaregion, India," J. Earth Syst. Sci, 116 (3), pp. 245–259, 2007.
[7] Y.N. Belevtsev, R.Y. Belevtsev, R.I. Siroshtan, "The Krivoy Rog Basin," A.F. Trendall, R.C. Morris, eds., Iron-Formation : Facts and Problems. Elsevier, Amsterdam, pp. 211–252, 1982
[8] N.N. Chombong, C.E. Suh, "2883 Ma commencement of BIF deposition at the northern edge of Congo craton, southern Cameroon: new zircon SHRIMP data constraint from metavolcanics," Episodes 36, pp. 47–57, 2013
[9] N.N. Chombong, C.E. Suh, B. Lehmann, A. Vishiti, D.C. Ilouga, E.M. Shemang, B.S. Tantoh, A.C. Kedia, 2017. "Host rock geochemistry, texture and chemical composition of magnetite in iron ore in the Neoarchaean Nyong unit in southern Cameroon," Appl. Earth Sci. http://dx.doi.org/10.1080/03717453.2017.1345507. 2017.
[10] J.H. Choi, and Y. Hariya, "Geochemistry and depositional environment of Mn Oxide deposits in the Tokoro Belt, Northeastern Hokkaido," Econ. Geol., 87, pp. 1265–1274, 1992
[11] P. Cloud, "Paleoecological significance of banded iron-formation," Economic Geology 68, 1135−1143, 1973
[12] H. Elderfield, and R. Pagett, "REE in ichthyoliths: Variations with redox conditions and depositional environment," In the Science of the Total Environment 49, pp. 175–197, 1986.
[13] J.L. Feybesse, V. Johan, P. Maurizot, A. Abessolo, "Mise en evidence d'une nappe syn métamorphe d'âge Eburnéen dans la partie Nord-Ouest du craton zaïrois, Sud-Ouest Cameroun,". In: Les formations birrimiennes en Afrique de l'Ouest, journée scientifique, compte rendu de conférences. Occasional Publications-CIFEG, pp. 105–111, 1986
[14] J.L. Feybesse, V. Johan, C. Triboulet, C. Guerrot, F. Mayaga-Mikolo, V. Bouchot, and J. Ekondong, "The West Central African belt: A model of 2.5-2.0 Ga ac- cretion and two-phase orogenic evolution" Precambrian Research, 87, pp. 161-216, 1998
[15] S. Ganno, T. Ngnotue, G.D. Kouankap Nono, J.P. Nzenti, F.M. Notsa, "Petrology and geochemistry of the banded iron-formations from Ntem complex greenstones belt, Elom area, Southern Cameroon: implications for the origin and depositional environment," Chem. Erde 75, pp. 375–387, 2015b
[16] S. Ganno, C. Moudioh, A. Nzina Nchare, G.D. Kouankap Nono, J.P. Nzenti, "Geochemical fingerprint and iron ore potential of the siliceous itabirite from palaeoproterozoic Nyong series, Zambi area, southwestern Cameroon," Resour. Geol. 66 (1), pp. 71–80, 2015a
[17] S. Ganno, Njiosseu E.L. Tanko, G.D. Kouankap Nono, A. Djoukouo Soh, C. Moudioh, T. Ngnotué, J.P. Nzenti, "A mixed seawater and hydrothermal origin of superior- type banded iron formation (BIF)-hosted Kouambo iron deposit, Palaeoproterozoic Nyong series, Southwestern Cameroon: Constraints from petrography and geochemistry," Ore Geol. Rev. 80, pp. 860–875, 2017
[18] S. Ganno, D. Tsozué, G.D. Kouankap Nono, M.S. Tchouatcha, T. Ngnotué, R. Gamgne Takam, J.P Nzenti, "Geochemical constraints on the origin of mineralized banded iron formation from the Meyomessi area, Archaean Ntem Complex (Congo Craton), southern Cameroon," Resour. Geol. http://dx.doi.org/10.1111/rge.12172. 2018.
[19] G.J.S. Govett, "Origin of Banded Iron-Formation," Geological Society of America Bulletin, 77, p. 1191-1212. 1966. https://doi.org/10.1130/0016-7606(1966)77[1191:OOBIF]2.0.CO2
[20] G.A. Gross, "A classification of iron formations based on depositional environments," Can. Mineral. 18, pp. 215–222, 1980
[21] T. Hamade, K.O. Konhauser, R. Raiswell, S. Goldsmith and R. C. Morris, "UsingGe/Si ratios to decouple iron and silica fluxes in Precambrian banded iron formations," Geology, 31, pp. 35– 38, 2003
[22] M.M. Herron, "Geochemical classification of terrigenous sands and shales from core or log data," J. Sediment. Petrol. 58, pp. 820–829, 1988
[23] D.L. Huston, G.A. Logan, "Barite, BIFs and bugs: evidence for the evolution of the Earth's early hydrosphere," Earth Planet. Sci. Lett. 220, pp. 41–55, 2004.
[24] C.D.I. Ilouga, C.E. Suh, R.T. Ghogomu, "Textures and rare earth elementscomposition of Banded Iron Formations (BIF) at Njweng prospect, Mbalam IronOre District, Southern Cameroon," Int. J. Geosci. 4, pp. 146–165, 2013
[25] D.C. Ilouga, Ndong F, Bidzang, L. Ziem A Bidias, J.B. Olinga, E. Tata, D. Minyem, "Geochemical Characterization of a Stratigraphic Log Bearing

Iron Ore in the Sanaga Prospect, Upper Nyong Unit of Ntem Complex," CameroonJournal of Geosciences and Geomatics, 2017, Vol. 5, No. 5, pp. 218-228, 2017. DOI:10.12691/jgg-5-5-1

[26] H.L. James, "Sedimentary facies of iron-formations," Econ. Geol. 49, pp. 235–293, 1954

[27] H.L. James, "Chemistry of the iron-rich sedimentary rocks," M. Fleischer, ed., Data of Geochemistry', 6th edition, Paper 440-W, U.S. Govt. Printing Office, Washington D.C, 1966

[28] H.L. James, "Precambrian iron-formations: Nature, origin, and mineralogic evolution from sedimentation to metamorphism," K.H. Wolf and G.V. Chilingarian, eds., DIAGENESIS III: Developments in Sedimentology, vol. 47. pp. 543–589, 1992.

[29] B. Kankeu, R.O. Greiling, J.P. Nzenti, S. Ganno, P.Y.E. Danguene, J. Bassahak, J.V Hell,. "Contrasting Pan-African structural styles at the NW margin of the Congo Shield in Cameroon," J. Afr. Earth Sci. http://dx.doi.org/10.1016/j.jafrearsci.2017.06.002. 2017.

[30] C. Klein, "Some Precambrian banded iron-formations (BIFs) from around the world: their age, geologic setting, mineralogy, metamorphism, geochemistry, and origin,"*Am. Mineral*, 90, pp. 1473–1499, 2005.

[31] C. Klein, N.J. Beukes, "Sedimentology and geochemistry of glaciogenic Late Proterozoic Rapitan iron-formation in Canada," Econ. Geol. 88, 542–565, 1993

[32] T.G. Lan, H.R. Fan, F.F. Hu, K.F. Yang, Y.C. Cai, Y.S. Liu, "Depositional environment and tectonic implications of the Paleoproterozoic BIF in Changyi area, eastern North China Craton: Evidence from geochronology and geochemistry of the metamorphic wallrocks," Ore Geol. Rev. 61, 52–72, 2014

[33] M. Lasserre, D. Soba, "Age Librrien des granodiorites et des gneiss à pyroxène du Cameroun Méridional," Bull. B.R.G.M. 2, pp. 17–32, 1976

[34] H. Lepp, and S.S. Goldich, Origin of the Precambrian Iron-Formation. Economic Geology, 59, pp. 1025-1060. https://doi.org/10.2113/gsecongeo.59.6.1025. 1964.

[35] C. Lerouge, A. Cocherie, S.F. Toteu, J. Penaye, J.P. Milesi, R. Tchameni, N.E. Nsifa, C.M. Fanning, E. Deloule, " Shrimp U/Pb zircon age evidence for Paleoproterozoic sedimentation and 2.05 Ga syntectonic plutonism in the Nyong Group, South-western Cameroon: consequences for the eburnean–transamazonian belt of NE Brazil and central Africa," J. Afr. Earth Sc. 44, 413–427, 2006.

[36] T.W. Lyons, C.T. Reinhard, N.J. Planavsky, "The rise of oxygen in the Earth's Early Ocean and atmosphere," Nature, V. 406, pp. 307-315, 2014

[37] V. Madaha Kodjo "Pretrographic and structural characterization of the Kribi-Campo fault in Fifinda-Londji area," DIPES II Dissertation, Univ. Bamenda, Cameroon, 2016.

[38] C. Manikyamba, S.M. Naqvi, "Geochemistry of Fe–Mn formations in theArchean Sandur schist belt, India: mixing of clastic and chemical processes at ashallow shelf," Precambrian Res. 72, 69–95, 1995.

[39] V. Marchig, H. Gundlach, P. Möller, F. Schley, "Some geochemical indicatorsfor discrimination between diagenetic and hydrothermal metalliferoussediments," Mar. Geol. 50, 241–256, 1982

[40] P. Maurizot, A. Abessolo, J.L. Feybesse, L.P. Johan, "Étude de prospection minière du Sud-Ouest Cameroun. Synthèse des travaux de 1978 à 1985," Rapport de BRGM 85, 274. 1986.

[41] P. Maurizot, "Geological map of south-west Cameroon," Edition BRGM, Orleans. 2000

[42] B.M. Mbang Bonda, J. Etame, A.P. Kouske, E.C. Bayiga, G.F. Ngon Ngon, S.J. Mbaï, M. Gérard, "Ore Texture, Mineralogy and Whole Rock Geochemistry of the Iron Mineralization from Edea North Area, Nyong Complex, Southern Cameroon: Implication for Origin and Enrichment Process," International Journal of Geosciences, 8, pp. 659-677. https://doi.org/10.4236/ijg.2017.85036. 2017.

[43] S.M. McLennan, "Rare earth elements in sedimentary rocks: influence of provenance and sedimentary processes," B.R. Lipin, G.A. McKay, eds., Geochemistry and Mineralogy of Rare Earth Elements. Rev. Miner. Geochem. pp. 169–200, 1989

[44] A.M. Mloszewska, E. Pecoits, N.L. Cates, S.J. Mojzsis, J. O'Neil, L.J. Robbins, K.O. Konhauser, "The composition of earth's oldest iron formations: the Nuvvuagittuq Supracrustal Belt (Quebec, Canada)," *Earth Planet. Sci. Lett.*pp. 317–318, pp. 331–342, 2012

[45] R.C. Morris, "A Textural and Mineralogical Study of the Relationship of Iron Ore to Banded Iron Formation in the Hamersley Iron Province of Western Australia," Eco- nomic Geology, Vol. 75, No. 2, pp. 184-209, 1980. doi:10.2113/gsecongeo.75.2.184

[46] S.K. Mukherjee, "Petrography, Age (U–Pb zircon), Geochemical and Isotopic Studies of the Sawawin Banded Iron-formation (BIF), Northwestern Saudi Arabia: Implications for Understanding Neoproterozoic Climate Change," Ph.D. thesis, University of Texas at Dallas, 2008.

[47] JL. Ndema Mbongué, "Evolution tectono-metamorphique de la serie du Nyong à Edea et à Eseka," Thèse de doctorat Ph.D, Dept. des Sciences de la Terre., Université de Yaoundé I. Cameroon., 2016.

[48] J.L. Ndema, Mbongué, T. Ngnotue, C.D. Ngo Nlend, J.P. Nzenti, C.E. Suh, "Origin and evolution of the formation of the Cameroon Nyong Series in the western border of the Congo Craton," J. Geosci. Geomat. 2, pp. 62–75, 2014.

[49] E.N. Ndime, S. Ganno, L. Soh Tamehe, J.P. Nzenti, "Petrography, lithostratigraphy and major element geochemistry of Mesoarchean metamorphosed banded iron formation-hosted Nkout iron ore deposit, north western Congo craton, Central West Africa," Journal of African Earth Sciences xxx (xxxx) xxx–xxx, https://doi.org/10.1016/j.jafrearsci.2018.06.007. 2018.

[50] M.T., Nforba, C.E., Suh, K.V.K., Kabeyene, "Mbalam iron ore project, northernedge of the Congo craton, southeast Cameroon," R.J. Goldfarb, E.E. Marsh and E. Monecke, eds., Proceedings of the Society of Economic Geologists on the Challenge of Finding New Mineral Resources: Global Metallogeny, Innovative Exploration and New Discoveries, SEG Extended Abstracts. Colorado, G-22, 2010

[51] S. Owona, "Archaean, Eburnean and Pan-African Features and Relationships in Their Junction Zone in the South of Yaounde (Cameroon)," Ph.D. dissertation, University of Douala, Cameroon, 2008.

[52] E. Pecoits, M.K. Gingras, M.E. Barley, A. Kappler, N.R. Posth, K.O. Konhauser, "Petrography and geochemistry of the Dales Gorge banded iron formation: paragenetic sequence, source and implications for palaeo-ocean chemistry," Precambria n Res. 172, pp. 163–187, 2009

[53] N. Planavsky, A. Bekker, O.J. Rouxel, B. Kamber, A. Hofmann, A. Knudsen, W.T. Lyons, "Rare earth element and yttrium compositions of Archae-

an and Paleoproterozoic Fe formations revisited: new perspectives on the significance and mechanisms of deposition," *Geochim. Cosmochim. Acta* 74, pp. 6387-6405, 2010

[54] A. Pouclet, R. Tchameni, K. Mezger, M. Vidal, E.N. Nsifa, C.K. Shang, J. Penaye, "Archaean crustal accretion at the northern border of the Congo craton (South Cameroon). The charnockite-TTG link," Bull. Geol. Soc. Fr. 178, pp. 331–342, 2007

[55] B.P. Roser, R.J. Korsch, "Determination of tectonic setting of sandstone–mudstone suites using SiO2 content and K2O/Na2O ratio," J. Geol. 94, pp. 635–650, 1986

[56] J. Siivola, and R. Schmid, "List of Mineral Abbreviations. Recommen-dations by the IUGS Subcommission on the Systematics of Metamor-phic Rocks," Web version 01.02.2007; www.bgs.ac.uk.scmr/home.html

[57] L. Soh Tamehe, W. Chongtaoa, S. Ganno, J.S. Shaamu, G.D.Kouankap Nono, J.P. Nzenti, Y.B. Lemdjoue, L. Naing Htun, "Geology of the Gouap iron deposit, Congo craton, southern Cameroon: Implications for iron ore exploration," Geology Reviews 107, pp. 1097–1128, 2019. https://doi.org/10.1016/j.oregeorev.2019.03.034

[58] L. Soh Tamehe, T.M. Nzepang, W. Chongtao, S. Ganno, T. Ngnotue, N.G.D. Kouankap, S.J. Simon, J. Zhang, J.P. Nzenti, "Geology and geochemical constrains on the origin and depositional setting of the Kpwa–Atog Boga banded iron formations (BIFs), northwestern Congo craton, southern Cameroon," Ore Geol. Rev. 95, pp. 620–638, 2018

[59] C.E. Suh, A. Cabral, E.M. Shemang, L. Mbinkar, G.G.M. Mboudou, "Two contrasting iron-ore deposits in the Precambrian mineral belt of Cameroon, West Africa," *Explor. Min. Geol*. 17, pp. 197–207, 2008

[60] R. Tchameni, A. Pouclet, K. Mezger, N.E. Nsifa and J.P. Vicat "A Monozircon and Sm- Nd whole rock ages from the Ebolowa greenstone belts: Evidence for the terranes older than 2.9Ga in the Ntem Complex (Congo craton, South Cameroon)," J. Camer. Acad. Sci. 4, pp. 213-224, 2004.

[61] T. Teutsong, T.R.R. Bontognali, P.-D. Ndjigui, J.C. Vrijmoed, D. Teagle, M. Cooper, Vance, Derek, "Petrography and geochemistry of the Mesoarchean Bikoula banded iron formation in the Ntem complex (Congo craton), Southern Cameroon: implications for its origin," *Ore Geol. Rev*. 80, pp. 267–288, 2017

[62] S.F. Toteu, W.R. Van Schmus, J. Penaye, A. Michard, "New U-Pb and Sm–Nd data from north-central Cameroon and its bearing on the pre-PanAfrican history of Central Africa,".*Precambr. Res*. pp. 108, 45–73, 2001.

[63] S.M. Toteu, W.R. Van Schmus, J. Penaye, J.B. Nyobé, "U-Pb and Sm–Nd evidence of eburnean and pan African high grade metamorphism in Cratonic rock of southern Cameroon," *Precambr. Res*. 67, pp. 321–347, 1994.

[64] J.R. Toth, "Deposition of submarine crusts rich in manganese and iron," *GSA Bull*. 91 (1), pp. 44–54, 1980.

[65] J. Wright, H. Schrader and W. Holser, "Paleoredox variations in ancient oceans recorded by rare earth elements in fossil apatite," *Geochim. Cosmochim*. Acta 51, pp. 631–644, 1987